Learning Imaging Biomarker Trajectories from Noisy Alzheimer's Disease Data Using a Bayesian Multilevel Model

Neil P. Oxtoby[1], Alexandra L. Young[1], Nick C. Fox[2], The Alzheimer's Disease Neuroimaging Initiative*, Pankaj Daga[1], David M. Cash[2,1], Sebastien Ourselin[1], Jonathan M. Schott[2], and Daniel C. Alexander[1]

[1] Progression Of Neurodegenerative Disease Initiative, Centre for Medical Image Computing, Department of Computer Science, University College London, Malet Place, London, WC1E 6BT, UK
[2] Dementia Research Centre, Institute of Neurology, University College London, 8-11 Queen Square, London, WC1N 3AR, UK

Abstract. Characterising the time course of a disease with a protracted incubation period ultimately requires dense longitudinal studies, which can be prohibitively long and expensive. Considering what can be learned in the absence of such data, we estimate cohort-level biomarker trajectories by fitting cross-sectional data to a differential equation model, then integrating the fit. These fits inform our new stochastic differential equation model for synthesising individual-level biomarker trajectories for prognosis support. Our Bayesian multilevel regression model explicitly includes measurement noise estimation to avoid regression dilution bias. Applicable to any disease, here we perform experiments on Alzheimer's disease imaging biomarker data — volumes of regions of interest within the brain. We find that Alzheimer's disease imaging biomarkers are dynamic over timescales from a few years to a few decades.

1 Introduction

Dementia presents a significant societal and economic burden to an ageing population. Late-onset dementia is generally attributed to degenerative neurological diseases such as Alzheimer's disease (AD). Biomarkers (biological markers) are indicators of disease-specific changes which can be used to inform the diagnosis of AD [1]. While no single biomarker is dynamic over the entire disease progression, AD biomarker abnormality is hypothesised to occur in a disease-specific sequence determined by the maximum gradient [2]. Most investigations of this hypothesis have sought to correlate biomarker gradient/change with clinically-determined subject cognition: cognitively normal (CN), mild cognitive impairment (MCI), or diagnosed AD [3]. This approach provides a coarsely-graded ordering of biomarker abnormality. More finely-graded sequencing of biomarker abnormality events has been achieved using data-driven models of disease progression [4–6]. Such models can be useful for diagnosis/staging of a patient, but accurate prognosis requires more complete knowledge of biomarker trajectories.

* ADNI See p. 93.

M.J. Cardoso et al. (Eds.): BAMBI 2014, LNCS 8677, pp. 85–94, 2014.

Characterising biomarker dynamics ultimately requires long-term, dense, longitudinal studies. Such data is expensive and difficult to obtain, whereas cross-sectional (or short-term longitudinal) data is relatively inexpensive, easy to obtain, and already available. For example, the Alzheimer's Disease Neuroimaging Initiative (ADNI) dataset. In this study we present a principled approach to quantitative biomarker dynamics. We start by estimating cohort-level (average) biomarker trajectories by integrating a parametric ordinary differential equation model which is fit to single-followup cross-sectional data, such as done in similar previous work [7–10, 19]. We innovate on previous work in two ways: 1) modelling (and estimating from the data) biomarker measurement noise using a Bayesian multilevel model (BMM); and 2) introducing a stochastic differential equation model for synthesising future biomarker trajectories of individuals, thus providing predictive/prognostic information. We describe the data and methods in Section 2, present results in Section 3, and discuss in Section 4.

2 Data and Methods

From ADNI-1* we consider a cross section of differential data $(x, y \equiv dx/dt)$ for each of five imaging biomarkers (see table 1). Here x is the baseline biomarker value (volume of a region of interest) and y is the forward finite-difference approximation of the derivative from baseline to 12-months. The regional brain volumes are normalised by intracranial volume [11] and presented as percentages. We focus our experimental results on only one region of interest, choosing the ventricles. Results for the other brain volumes are summarised. To maintain specificity to disease progression we included the entire cognitive spectrum except for non-stable or non-progressing individuals (mixed or regressing diagnoses). Excluding individuals with missing data left $N = 651$ individuals.

Illustrative Example of our Approach. Figure 1 illustrates the pipeline of our approach using ventricles data. The single-followup data in figure 1a produces a differential cross section, which is fit to a polynomial differential equation in figure 1b. Integrating the differential equation produces the cohort-level trajectory in figure 1c. The solid blue line shows the average, with dotted and dashed red lines respectively showing short and long transitions from the ± 1 standard error bounds on the model parameter estimates. Figure 1d shows individual-level trajectories synthesised by a stochastic differential equation. We proceed now to present details of our methodology.

Regression Model. For each biomarker $x(t)$ we performed model selection using the sample-size-corrected Akaike information criterion. For this purpose we used ordinary least squares (OLS) differential equation models $y = f(x)$, with polynomials $f(x)$ of up to second-order, as well as linear dependence on mean-centred covariates — age and education. We considered group differences by sex, and performed a separate regression for the whole cohort and for the apoE4+ subcohort of genetic risk factor carriers (apoE4 = apolipoprotein-E4). Of the $N = 651$ stable or progressing individuals with suitable brain volumetry data in ADNI-1, 321 were apoE4+ (had one or more apoE4 alleles). Distinct

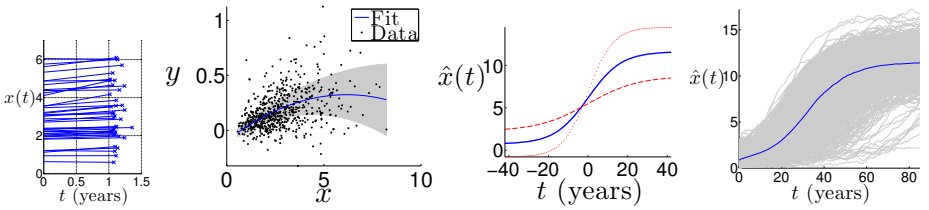

(a) Data **(b)** Differential fit **(c)** Est. trajectory **(d)** Stochastic model

Fig. 1. Pipeline illustrated on ventricles: (a) single-followup cross-section; (b) differential equation fit; (c) cohort-level trajectory; (d) individual synthetic trajectories (see also figure 3).

from previous work, we use a multilevel differential equation model that incorporates additive Gaussian noise on the biomarker observations $\tilde{x}(t) = x(t) + \eta(t)$. In general, the Gaussian random variable $\eta \sim \mathcal{N}(0, \sigma_z^2)$ may exhibit longitudinal correlation, but since cross-sectional data cannot support estimation of such intra-subject variance, we assume the measurement noise autocorrelation coefficient $\rho(t-s) \equiv \mathrm{E}\left[\eta(t)\eta(s)\right]/\sigma_z^2$ to be $\rho = 0$. (We retain ρ in the covariance matrix below for completeness.)

Our multilevel model has three levels: dynamics (one data point per *i*ndividual), one group level to capture sex differences ($s[i]$), and additive Gaussian measurement noise:

$$\begin{aligned} y_i &\sim \mathcal{N}\left(f(x_i, \boldsymbol{\mu}_{s[i]}), \sigma_y^2\right) \\ \begin{pmatrix} \tilde{x}_i \\ \tilde{y}_i \end{pmatrix} &\sim \mathcal{N}\left(\begin{pmatrix} x_i \\ y_i \end{pmatrix}, \Sigma\right) \end{aligned} \tag{1}$$

where polynomial $f(x, \boldsymbol{\mu})$ is the dynamical model (see below) parametrised by the vector $\boldsymbol{\mu}$ of sex-specific fixed effects and σ_y^2 is residual model error (unexplained variance). The finite-difference derivative $y_i \approx (x_i(T_i) - x_i(0))/T_i$ is correlated with $x_i = x_i(0)$ giving the measurement covariance structure

$$\Sigma_i = \sigma^2 \begin{bmatrix} 1, & -(1-\rho)/T_i \\ -(1-\rho)/T_i, & 2(1-\rho)/T_i^2 \end{bmatrix} \tag{2}$$

where we assume zero intra-subject autocorrelation as discussed above, so $\rho = 0$. The precise value of T_i is used (nominally $T = 1$ year).

Our Bayesian multilevel models are fit numerically using Markov Chain Monte Carlo (MCMC) techniques. For this purpose we used the Stan [12] software package. Full validation is a topic for future work, but it is reassuring to note that we found similar results using the JAGS [13,14] software package. We contrast our results with those obtained using OLS. To ensure that the estimation was driven by the data, our Bayesian models used weakly-informative priors: broad Gaussian priors ($\sigma \geq 100$) for regression parameters and broad positive uniform priors (upper bound $10\tilde{x}_{\max}$) for the variance parameters. We tried different weakly-informative priors (e.g., inverse gamma priors for variances) and the results were unchanged, giving us confidence that the data was driving our inference.

Cohort-level Biomarker Trajectories. Each cohort-level biomarker trajectory is ultimately determined by the (unknown) disease stage for each subject, and represented within our model by the regression parameter estimates. Linear fits produce exponential trajectories, where $f(x) = \mu_{0,s[i]} + \mu_{1,s[i]}x + \mu_{3,s[i]} \cdot \text{age} + \mu_{4,s[i]} \cdot \text{edu}$. This corresponds to acceleration or deceleration/saturation of atrophy in the brain. Quadratic fits, where $f(x) = \mu_{0,s[i]} + \mu_{1,s[i]}x + \mu_{2,s[i]}x^2 + \mu_{3,s[i]} \cdot \text{age} + \mu_{4,s[i]} \cdot \text{edu}$, are a parsimonious representation of sigmoidal trajectories (acceleration followed by deceleration). We note the following convenient analytical form for a sigmoidal trajectory

$$x(t) = x_- + \frac{\Delta}{1 + e^{-rt}} \tag{3}$$

where r is a biomarker progression rate, and $\Delta \equiv x_+ - x_-$ separates the asymptotes $x_\pm \equiv x(t = \pm\infty)$ which bound the sigmoid. Time t is symmetric about the primary inflection point $x(t = 0) = x_- + \Delta/2$, and is unrelated to study/visit time (since baseline). The sigmoid parameters are straightforward functions of the regression parameters $\boldsymbol{\mu}$. We will utilise equation (3) to define a timescale of interest for the cohort (see equation (4) in section 3).

Individual-level Biomarker Trajectories. The ordinary differential equation reflects biomarker dynamics at the cohort level. We model individual-level biomarker dynamics as deviations about this average using a corresponding stochastic differential equation driven by a zero-mean Gaussian process $d\kappa \sim GP(0, \sigma_\kappa^2)$. We propose a prognostic utility for this below.

Biomarker Abnormality Timescales. Model fitting is followed by estimation of a biomarker abnormality timescale for the cohort, and one for individuals. The first is a cohort-level estimate of the duration over which the biomarker is dynamic: between two extremal thresholds $x_\text{s}(t_\text{s})$ (effective *s*aturation) and $x_\text{a}(t_\text{a})$ (initial signs of *a*bnormality). Choosing these thresholds is an open problem. For sigmoidal trajectories we choose analytical thresholds: the points of maximum biomarker acceleration and deceleration. For exponential trajectories (biomarker timescales not presented here) we propose using thresholds of clinical relevance. The second timescale uses our stochastic model to estimate an analogous result for an individual j. Starting at the individual's initial measurements $(\tilde{x}_j, \tilde{y}_j)$, many stochastic trajectories are synthesised using the deviation from the cohort fit as the Gaussian process scale $\sigma_{\kappa,j} = |\tilde{y}_j(\tilde{x}_j) - \hat{y}_\text{fit}(\tilde{x}_j)|$, and sampling model parameters $\boldsymbol{\mu}_j$ from the posterior distributions of the cohort-level multilevel regression parameters. The average of these synthetic trajectories for an individual gives a density of first-passage times (see [15]) taken to reach some maximal threshold, e.g., the effective saturation threshold in the case of biomarker saturation. This is an interval estimate of time remaining until an individual's biomarker becomes fully abnormal, which can inform prognosis either on it's own, or as part of a panel of such times for multiple biomarkers.

3 Results

MCMC. The Bayesian Multilevel Model (BMM) fitting converged using 2 chains, 2000 burn-in samples, and 8000 MCMC samples, thinned by 2. That is, we observed Gelman's potential scale reduction factor [16] to be $PSRF < 1.1$ for all parameters and hyperparameters, as well as observing all Monte Carlo standard errors to be lower than the posterior standard deviations.

Regression. As expected, our BMM produces different results to OLS — for example, the different quadratic regression fits shown for ventricles in figure 2a (males and females were pooled together in this figure). Multilevel regression parameter estimates for $\boldsymbol{\mu}$ are in table 1. The only data supporting a sigmoidal

Table 1. Multilevel regression fit results: mean (±std) $\times 10^{-3}$. ADNI-1 data at baseline and 12 months were available for $N = 651$ (370 male) stable or progressing subjects – of these, 321 (185 male) were apoe4+ subjects. Sex-specific regression parameters are $\mu_{k,s}$ with $k = 0, 1, 2$ (polynomial coefficients) and $s = m, f$ (male,female).

Biomarker, x	$\mu_{0,m}$	$\mu_{0,f}$	$\mu_{1,m}$	$\mu_{1,f}$	$\mu_{2,m}$	$\mu_{2,f}$	σ
Ventricles – all	−126 (52)	−81 (58)	166 (31)	122 (44)	−17 (4)	−6 (8)	9 (4)
– apoE4+	−174 (75)	−76 (94)	214 (42)	123 (73)	−23 (5)	−3 (13)	
Hippocampus – all	−19 (5)	−20 (6)	29 (14)	21 (15)	n/a	n/a	6 (2)
– apoE4+	−17 (8)	−17 (9)	−19 (23)	11 (24)	n/a	n/a	
Entorhinal cortex – all	−0.4 (4)	−10 (4)	−26 (16)	8 (20)	n/a	n/a	2 (1)
– apoE4+	4.9 (5.1)	−13 (7)	−59 (24)	25 (32)	n/a	n/a	
Fusiform – all	−28 (21)	−47 (23)	2 (20)	21 (21)	n/a	n/a	8 (3)
– apoE4+	−13 (30)	−55 (31)	−21 (29)	24 (29)	n/a	n/a	
Mid. temp. gyrus – all	−39 (24)	−56 (28)	7 (20)	22 (23)	n/a	n/a	10 (3)
– apoE4+	−48 (34)	−39 (40)	5 (29)	4 (34)	n/a	n/a	

Table 2. Ordinary least squares fit results: mean (±std) $\times 10^{-3}$. Compare with multilevel regression results in Table 1.

Biomarker, x	μ_0	μ_1	μ_2
Ventricles – all	−41 (62)	72 (46)	−3 (8)
– apoE4+	−92 (96)	130 (72)	−7 (12)
Hippocampus – all	−16 (7)	21 (17)	n/a
– apoE4+	−19 (10)	20 (26)	n/a
Entorhinal cortex – all	−10 (5)	16 (22)	n/a
– apoE4+	−19 (7)	52 (33)	n/a
Fusiform – all	−50 (29)	33 (26)	n/a
– apoE4+	−64 (37)	38 (35)	n/a
Mid. temp. gyrus – all	−16 (33)	0 (27)	n/a
– apoE4+	−22 (45)	−5 (37)	n/a

trajectory was the ventricles of males. The corresponding parameters for equation (3) are shown in Table 3. In both tables, estimates (posterior means) exceeded in magnitude by their standard errors (posterior standard deviations) are effectively zero. From this we can infer the biomarkers for which this combination of data and model implies undetectable change. Acceleration in hippocampal atrophy was detected for the stables/progressors, but not for the apoE4+ subset. Deceleration of atrophy was detectable in the entorhinal cortex of males, but not in females. And for the other regions of interest (fusiform and middle temporal gyrus), this combination of data and model implied undetectable change.

Focussing on ventricles, figure 2b overlays the OLS parameter estimates (vertical lines) upon histograms of the MCMC samples from the BMM. The OLS results differ considerably from the BMM results in value and confidence (spread), resulting in considerably different estimates of the dynamic duration for the biomarker: $\tau = 19 \pm 6$ years (BMM) versus $\tau = 33 \pm 26$ years (OLS). We hypothesize that the BMM has removed a bias present in the OLS regression estimate due to ignoring the measurement noise present in x. The lower right of figure 2b shows a histogram for the measurement noise scale σ from equation (2), compared to the offline estimate from stable controls (red line), which appears to be an overestimate.

We note that there were differences between males and females. The most impressive were for the entorhinal cortex, where the linear differential equation gradients had different signs. Further investigation would require more data and perhaps modelling, so we relegate it to future work.

Our estimates of the Gaussian measurement noise "size" (standard deviation) were all of the order of $\sigma \sim 10^{-3} \approx 0.1\%$ of intracranial volume. This represented between one-third and one-half of the model residual size σ_y.

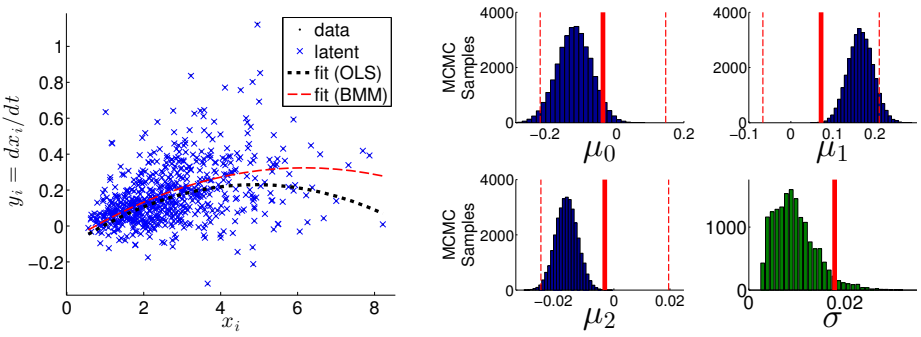

(a) Multilevel model fits **(b)** Model parameter estimates

Fig. 2. Regression results for ventricles. Histograms for the multilevel fit parameter MCMC samples are shown with overlays (red lines) of the complete pooling regression results for $\mu_k \pm 3$ standard error. The measurement noise histogram (lower right; green) is compared with the variance in ADNI-1 stable control ventricles measurements, averaged across individuals.

Table 3. Sigmoid parameters and biomarker dynamic duration results for the ventricles of males

Biomarker, x	r, per year	x_-	x_+	x_a	x_s	τ, years
Ventricles (males) – BMM	0.14 (0.04)	0.8 (0.9)	8.9 (1.4)	2.5	7.2	19 (6)
Ventricles (males) – OLS	0.081 (0.065)	0.7 (2.6)	8.8 (4.0)	2.4	7.1	33 (26)

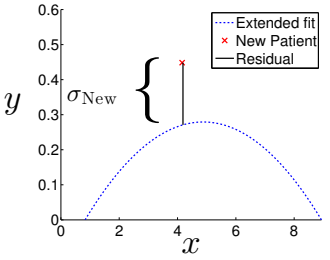

(a) New patient: deviation from cohort

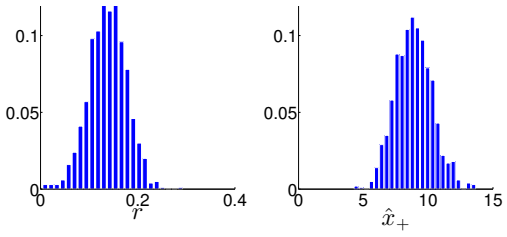

(b) Parameter histograms

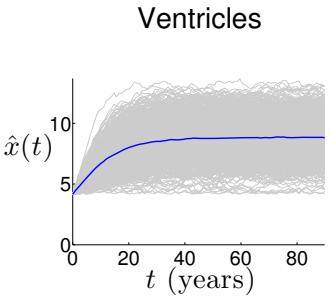

(c) Sample paths

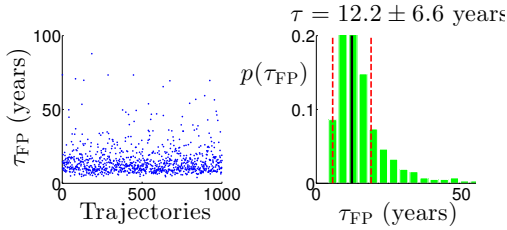

(d) First-passage times

Fig. 3. Prognostic utility of our approach: stochastic model. See text for details.

Cohort-level Biomarker Abnormality Timescale. For sigmoidal dynamics, our analytical thresholds for initial abnormality and effective saturation (points of maximal acceleration and deceleration) are found by using equation (3) and solving $dx^3/dt^3 = 0$. The time interval between these thresholds is

$$\tau = \frac{1}{r} \ln \left(\frac{2 + \sqrt{3}}{2 - \sqrt{3}} \right) . \tag{4}$$

We found $\tau = 19 \pm 6$ years for ventricles in males (the only data to support a sigmoidal trajectory). For exponential biomarker trajectories (not presented here), clinically-relevant thresholds would be appropriate for estimating τ.

Individual-level Biomarker Abnormality Timescale. We calculated the biomarker effective saturation time for the ventricle volume of a randomly-selected individual (RID=1384; diagnosed MCI) at visits not included in the

original fit (to avoid circularity): 24 and 36 months. This data point and the resulting residual are shown with the pre-existing cohort fit in Figure 3a. The model parameters sampled from the BMM posterior distributions shown in Figure 3b were used to synthesise the 1000 trajectories in Figure 3c. The corresponding first-passage times are shown in Figure 3d. Due to the long tail of the distribution, we used robust statistics (median ± median absolute deviation) to calculate the biomarker effective saturation time as $\tau_{\mathrm{FP}} = 12.2 \pm 6.6$ years from a ventricular volume of $x_j = 4.1\%$ to the saturation threshold of $x_{\mathrm{s}} = 8.9\%$ (percentage of intracranial volume).

4 Discussion

Neurodegeneration causes the ventricles to expand and all other brain volumes to decline. Measurement noise and intra-subject variability confound this, e.g., some progressing individuals display $y > 0$ even for brain volumes which should be in decline. Indeed, the apparent bias in OLS results suggests that measurement noise should be modelled in a differential equation approach. Quantitatively we found that ventricles saturated after an expansion lasting approximately two decades. This timescale is consistent with current knowledge of Alzheimer's disease, and related work on biomarker trajectories [10, 17, 19].

We found low coefficients of determination $R^2 \leq 0.33$, as in related work [10], implying that a small proportion of the variance in the data was explained by the model. This is not particularly surprising for two reasons: 1) cross-sectional data cannot be used to distinguish between inter-subject and intra-subject variance; and 2) the simplicity of the model compared with the unknown complexity of Alzheimer's disease. For example, the observations in ADNI-1 of hippocampal growth (or ventricular contraction) in diseased subjects could be a consequence of intra-subject variation on the relatively short timescale used to calculate biomarker change (~ 1 year compared to the decades-long incubation period). A first step to reduce the influence of such intra-subject variance (not considered here) would be to use the entire set of followup data from ADNI. Given enough data points per individual, inter-subject variance and heteroscedasticity could be explicitly modelled and estimated. There is hope that dense longitudinal data, as it becomes available, will allow fitting of more complex models that explain the data better.

This study addressed an important problem: how to infer information about disease biomarker trajectories from noisy cross-sectional data, which is readily-available and relatively inexpensive. Cohort-level trajectories were estimated by fitting an ordinary differential equation model, and integrating the fit. Individual-level trajectories were modelled as Gaussian deviations from the cohort using a stochastic differential equation model, allowing trajectory synthesis to inform prognosis. We innovated over previous differential equation models in two ways. First by using a Bayesian multilevel regression model to separately identify measurement noise and population variance. Our second innovation was the stochastic model. The Bayesian multilevel model avoids biassed parameter estimates, which can arise due to regression dilution. Experiments were performed

on Alzheimer's disease imaging data from the ADNI. We presented full results only for ventricle volume (a quadratic differential equation with sigmoidal time course), but our framework is not limited to a particular dynamical model.

In conclusion, clinicians focussing on patient outcomes ultimately desire improved diagnosis and prognosis — informed by biomarkers, including those derived from medical image computing. Prognostic uncertainty can be as important to the patient as the prognosis itself [18], so it is crucial to provide interval estimates of relevant time scales where possible. Our stochastic model allows interval estimation of the time remaining until a biomarker approaches maximal abnormality. A panel of such estimates for multiple biomarkers could be used to inform prognosis, e.g., estimation of time until onset of dementia. In the future we envisage developing such a prognostic tool using our approach in concert with disease progression models and/or longitudinal quantitative tools such as recurring-event survival analysis.

*Data used in preparation of this article was obtained from the ADNI database (`adni.loni.usc.edu/`). As such, the investigators within the ADNI contributed to the design and implementation of ADNI and/or provided data but did not participate in analysis or writing of this report. A complete listing of ADNI investigators can be found at `http://adni.loni.usc.edu/wp-content/uploads/how_to_apply/ADNI_Acknowledgement_List.pdf`. Funding for the ADNI project came from National Institutes of Health Grant U01 AG024904. Further details of funding for the ADNI are available via the ADNI website: `www.adni-info.org`.

References

1. McKhann, G.M., Knopman, D.S., Chertkow, H., Hyman, B.T., Jack Jr., C.R., Kawas, C.H., Klunk, W.E., Koroshetz, W.J., Manly, J.J., Mayeux, R., Mohs, R.C., Morris, J.C., Rossor, M.N., Scheltens, P., Carrillo, M.C., Thies, B., Weintraub, S., Phelps., C.H.: The diagnosis of dementia due to Alzheimer's disease: Recommendations from the National Institute on Aging-Alzheimer's Association workgroups on diagnostic guidelines for Alzheimer's disease. Alzheimer's & Dementia 7(3), 263–269 (2011)
2. Jack, C.R., Knopman, D.S., Jagust, W.J., Shaw, L.M., Aisen, P.S., Weiner, M.W., Petersen, R.C., Trojanowski, J.Q.: Hypothetical model of dynamic biomarkers of the Alzheimer's pathological cascade. The Lancet Neurology 9(1), 119–128 (2010)
3. Weiner, M.W., Veitch, D.P., Aisen, P.S., Beckett, L.A., Cairns, N.J., Green, R.C., Harvey, D., Jack, C.R., Jagust, W., Liu, E., Morris, J.C., Petersen, R.C., Saykin, A.J., Schmidt, M.E., Shaw, L., Siuciak, J.A., Soares, H., Toga, A.W., Trojanowski, J.Q.: The Alzheimer's Disease Neuroimaging Initiative: A review of papers published since its inception. Alzheimer's & Dementia 8(1), S1–S68 (2012)
4. Fonteijn, H.M., Modat, M., Clarkson, M.J., Barnes, J., Lehmann, M., Hobbs, N.Z., Scahill, R.I., Tabrizi, S.J., Ourselin, S., Fox, N.C., Alexander, D.C.: An event-based model for disease progression and its application in familial Alzheimer's disease and Huntington's disease
5. Huang, J., Alexander, D.: Probabilistic Event Cascades for Alzheimer's disease. In: Advances in Neural Information Processing Systems, pp. 3104–3112 (2012)

6. Young, A.L., Oxtoby, N.P., Daga, P., Cash, D.M., Fox, N.C., Ourselin, S., Schott, J.M., Alexander, D.C.: A data-driven model of biomarker changes in sporadic Alzheimer's disease. Brain 137(9), 2564–2577 (2014), http://brain.oxfordjournals.org/content/137/9/2564
7. Ashford, J.W., Schmitt., F.A.: Modeling the time-course of Alzheimer dementia. Current Psychiatry Reports 3(1), 20–28 (2001)
8. Yang, E., Farnum, M., Lobanov, V., Schultz, T., Raghavan, N., Samtani, M.N., Novak, G., Narayan, V., DiBernardo, A.: Quantifying the Pathophysiological Timeline of Alzheimer's Disease. Journal of Alzheimer's Disease 26(4), 745–753 (2011)
9. Sabuncu, M., Desikan, R., Sepulcre, J., Yeo, B., Liu, H., Schmansky, N., Reuter, M., Weiner, M., Buckner, R., Sperling, R.: The dynamics of cortical and hippocampal atrophy in Alzheimer disease. Archives of Neurology 68(8), 1040 (2011)
10. Villemagne, V.L., Burnham, S., Bourgeat, P., Brown, B., Ellis, K.A., Salvado, O., Szoeke, C., Macaulay, S.L., Martins, R., Maruff, P., Ames, D., Rowe, C.C., Masters, C.L.: Amyloid β deposition and neurodegeneration and cognitive decline in sporadic Alzheimer's disease: a prospective cohort study. The Lancet Neurology 12(4), 357–367 (2013)
11. Barnes, J., Ridgway, G.R., Bartlett, J., Henley, S.M.D., Lehmann, M., Hobbs, N., Clarkson, M.J., MacManus, D.G., Ourselin, S., Fox, N.C.: Head size, age and gender adjustment in MRI studies: a necessary nuisance? NeuroImage 53(4), 1244–1255 (2010)
12. Stan Development Team: Technical report, Stan: A C++ Library for Probability and Sampling, Version 2.2 (2014)
13. Plummer., M.: JAGS: A program for analysis of Bayesian graphical models using Gibbs sampling. In: Proceedings of the 3rd International Workshop on Distributed Statistical Computing (2003)
14. Steyvers, M.: Technical report MATJAGS 1.3, psiexp.ss.uci.edu/research/programs_data/jags
15. Jacobs, K.: Stochastic Processes for Physicists. Cambridge University Press (2010)
16. Gelman, A., Rubin, D.B.: Inference from iterative simulation using multiple sequences. Statistical Science 7(4), 457–472 (1992)
17. Villain, N., Chételat, G., Grassiot, B., Bourgeat, P., Jones, G., Ellis, K.A., Ames, D., Martins, R.N., Eustache, F., Salvado, O., Masters, C.L., Rowe, C.C., Villemagne, V.L., The AIBL Research Group: Regional dynamics of amyloid-β deposition in healthy elderly, mild cognitive impairment and Alzheimer's disease: a voxelwise PiB–PET longitudinal study. Brain 135(7), 2126–2139 (2013)
18. Smith, A.K., White, D.B., Arnold, R.M.: Uncertainty — the other side of prognosis. New England Journal of Medicine 368(26), 2448–2450 (2013)
19. Jack, C.R., Wiste, H.J., Lesnick, T.G., Weigand, S.D., Knopman, D.S., Vemuri, P., Pankratz, V.S., Senjem, M.L., Gunter, J.L., Mielke, M.M., Lowe, V.J., Boeve, B.F., Petersen, R.C.: Brain β-amyloid load approaches a plateau. Neurology 80(10), 890–896 (2013)